THE JOURNAL OF BIOLOGICAL CHEMISTRY VOL. 292, NO. 10, pp. 4034–4043, March 10, 2017

Coupling of Insulin Secretion and Display of a Granule-resident Zinc Transporter ZnT8 on the Surface of Pancreatic Beta Cells*

Received for publication, December 12, 2016, and in revised form, January 24, 2017 Published, JBC Papers in Press, January 27, 2017, DOI 10.1074/jbc.M116.772152

Qiong Huang[1], **Chengfeng Merriman, Hao Zhang, and Dax Fu**[2]

From the Department of Physiology, Johns Hopkins School of Medicine, Baltimore, Maryland 21205

Edited by Jeffrey E. Pessin

The islet-specific zinc transporter ZnT8 mediates zinc enrichment in the insulin secretory granules of the pancreatic beta cell. This granular zinc transporter is also a major self-antigen found in type 1 diabetes patients. It is not clear whether ZnT8 can be displayed on the cell surface and how insulin secretion may regulate the level of ZnT8 exposure to extracellular immune surveillance. Here we report specific antibody binding to the extracellular surface of rat insulinoma INS-1E cells that stably expressed a tagged human zinc transporter ZnT8. Flow cytometry analysis after fluorescent antibody labeling revealed strong correlations among the levels of ZnT8 expression, its display on the cell surface, and glucose-stimulated insulin secretion (GSIS). Glucose stimulation increased the surface display of endogenous ZnT8 from a basal level to 32.5% of the housekeeping Na^+/K^+ ATPase on the cell surface, thereby providing direct evidence for a GSIS-dependent surface exposure of the ZnT8 self-antigen. Moreover, the variation in tagged-ZnT8 expression and surface labeling enabled sorting of heterogeneous beta cells to subpopulations that exhibited marked differences in GSIS with parallel changes in endogenous ZnT8 expression. The abundant surface display of endogenous ZnT8 and its coupling to GSIS demonstrated the potential of ZnT8 as a surface biomarker for tracking and isolating functional beta cells in mixed cell populations.

The pancreatic beta cell is ranked among the most specialized cells in the human body, functioning as a sole source for providing insulin in response to the blood glucose level (1). After a meal, beta cells are stimulated not only to secrete insulin but also to replenish the intracellular insulin stores by up-regulation of proinsulin biosynthesis. As much as 20–50% of the total protein synthesized in a beta cell is proinsulin under stimulation conditions (2). Every six insulin molecules need two zinc ions to form a hexameric complex that is crystallized in the insulin secretory granules (3). As a result, pancreatic beta cells have one of the highest zinc concentrations among mammalian cells with estimated values between 10 to 20 mM in insulin granules (4). The granular zinc enrichment is mediated by a pancreatic zinc transporter, ZnT8 (5–8). Among known mammalian zinc transporters (9), ZnT8 is exquisitely unique in its tissue-specific expression (10). ZnT8 was found almost exclusively in pancreatic islets (11), mostly restricted to beta cells and to a lesser extent to non-beta endocrine cells (12–15). Moreover, the expression of ZnT8 in beta cells is predominantly localized to insulin granules (11) that undergo iterative cycles of exocytosis and membrane endocytosis to restore granule homeostatic abundance (16). During the exocytotic fusion events, selective but not all granular membrane proteins could laterally diffuse into the surface membrane (Fig. 1*A*) (17, 18). It is not clear, however, whether the granule-resident ZnT8 is linked to the insulin secretory pathway and how glucose stimulation may modulate the level of ZnT8 surface display.

The unique insulin biology of the beta cell requires specialized proteins like ZnT8 to support a high flux turnover of the insulin secretory pathway. Many of these proteins are potential targets of the immune system with implications for the etiology of type 1 diabetes (19–21), an autoimmune disease characterized by specific T-cell-mediated autoimmune destruction of pancreatic beta cells (22). Both $CD4^+$ and $CD8^+$ T-cell responses against ZnT8 (23–27) as well as anti-ZnT8 autoantibodies (28) were found in patients or model animals that developed autoimmune diabetes. Cell- or antibody-mediated autoimmune responses may be directly targeted at ZnT8 displayed on the beta cell surface either in a form of processed ZnT8 peptides associated with MHC class I molecules or intact ZnT8 self-antigen. Tracking the surface display of intact ZnT8 is the first step in closing a knowledge gap regarding how ZnT8 self-antigen may be exposed to extracellular immune surveillance before the onset of beta cell destruction. In particular, a putative coupling between the GSIS[3] and ZnT8 surface display may enforce a positive feedback loop of beta cell destruction, starting from a moderate initial beta cell loss to a compensatory increase of GSIS/ZnT8 exposure that exacerbates autoimmune insults and beta cell loss. As such, the coupling between GSIS and ZnT8 surfacing may contribute to a vicious cycle of disease

* This work was supported, in whole or in part, by National Institutes of Health Grant R01 GM065137. The authors declare that they have no conflicts of interest with the contents of this article. The content is solely the responsibility of the authors and does not necessarily represent the official views of the National Institutes of Health.

[1] Supported in part by National Natural Science Foundation of China Grant GP 81673492.

[2] To whom correspondence should be addressed: Dept. of Physiology, Johns Hopkins School of Medicine, 725 North Wolfe St., Baltimore, MD 21205. Tel.: 443-287-4941; E-mail: dfu3@jhmi.edu.

[3] The abbreviations used are: GSIS, glucose-stimulated insulin secretion; FSEC, fluorescence size exclusion HPLC; pAb, polyclonal antibody; DDM, dodecyl maltoside; KRBH, Krebs-Ringer bicarbonate HEPES.

progression to overt type 1 diabetes with an ultimate loss of beta cell mass and deterioration of glycemic control (29).

A critical technical barrier to tracking ZnT8 on the surface of live beta cells is the lack of a specific and sensitive ZnT8 tracer. Here, we report structure-guided tagging and specific immunofluorescence staining of ZnT8 on the extracellular surface of INS-1E cells (30) that stably expressed tagged ZnT8. Flow cytometry quantification of ZnT8 surface display revealed a sigmoidal correlation with GSIS. Further analysis of endogenous ZnT8 surfacing in clonal INS-1E cells demonstrated that ZnT8 was abundantly displayed on the cell surface in a GSIS-dependent fashion, thereby providing direct experimental evidence to link increased insulin secretion and ZnT8 self-antigen exposure. Moreover, specific antibody labeling of tagged-ZnT8 on the cell surface enabled flow cytometry sorting of heterogeneous INS-1E cells to subpopulations with varied GSIS phenotypes, suggesting that ZnT8 may be used as a surface biomarker for tracking and isolating functional beta cells in mixed cell populations.

Results

Design of an Antibody-ZnT8 Complex—The luminal face of a granular ZnT8 would be displayed on the cell surface if ZnT8 is translocated to the plasma membrane after insulin granule exocytosis (Fig. 1*A*). The X-ray structure of a bacterial ZnT8 homolog (YiiP) suggested that a ZnT8 homodimer adopts a Y-shaped immunoglobulin-like architecture (31, 32). This structural similarity may give rise to a specific and stable ZnT8-antibody complex through dual epitope-paratope recognition and interlock binding (Fig. 1*A*). Guided by homology modeling, we inserted an octapeptide FLAG epitope to the ZnT8 extracellular loops. In addition, we also added a green fluorescence protein (GFP) tag (33) to the cytosolic C terminus (Fig. 1*A*). The folding of the tagged-ZnT8 in the detergent extract of stably transfected INS-1E cells was examined by fluorescence size exclusion HPLC (FSEC). ZnT8 with a C-terminal GFP fusion tag (termed ZnT8-GFP) revealed a major monodispersed GFP fluorescence peak as reported previously (34). Inserting a FLAG epitope at one of the nine sites on the ZnT8 extracellular surface yielded only one tagged construct that exhibited a monodispersed FSEC profile. Structure modeling indicated that the FLAG epitope was inserted to the most exposed section of this doubly-tagged FLAG-ZnT8-GFP construct, termed ZnT8-FLAG/GFP (Fig. 1*A*).

Stable Expression of Tagged-ZnT8—Anti-GFP and anti-FLAG Western blotting confirmed the expression of ZnT8-GFP or ZnT8-FLAG/GFP in pooled stable INS-1E transfectants, corresponding to a major protein band between the 50 and 75 kDa markers (Fig. 1*B*). In contrast, anti-FLAG and anti-GFP signals were not detected in non-transfected INS-1E cells (Fig. 1*B*). Endogenous rat ZnT8 was detected by an anti-ZnT8 antibody, showing strong immunoblotting signals below the 50 kDa marker in both stably transfected and non-transfected INS-1E cells (*left panel*, Fig. 1*C*). The observed molecular mass between 45 and 50 kDa for rat ZnT8 (calculated $M_r = 40.1$ kDa) matched the manufacture's specification (Proteintech). On the same anti-ZnT8 blot, however, ZnT8-GFP and ZnT8-FLAG/GFP were barely detectable above the 50-kDa marker. Because

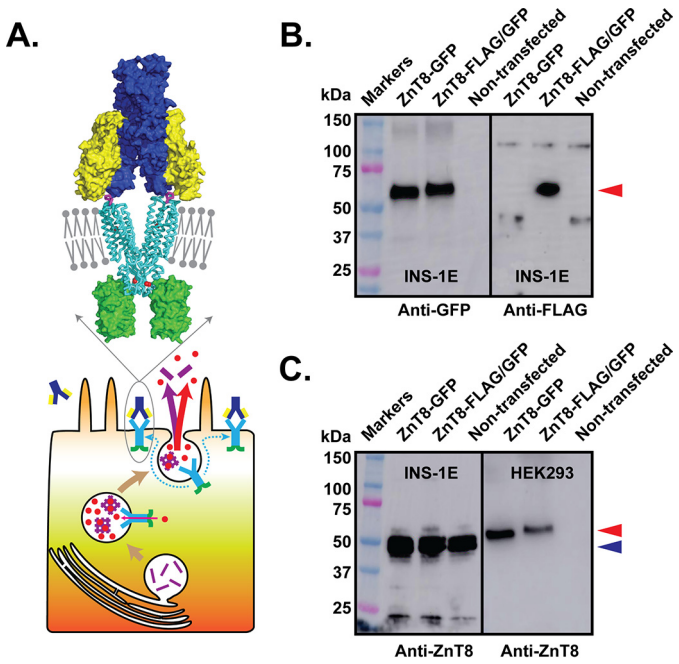

FIGURE 1. **Stable expression of tagged-ZnT8.** *A*, schematic diagram of the ZnT8 surface display after exocytosis of insulin secretory granules of a pancreatic beta cell with an enlarged view of a structural model of a ZnT8 homodimer (*cyan ribbon*) in the plasma membrane (*gray bars* and *balls*) in complex with a immunoglobin composed of two identical light chains (*yellow*) and heavy chains (*blue*) in surface representation. A pair of FLAG tags (*magenta sticks*) on the extracellular surface of ZnT8 mediates antibody binding. *Red spheres* are zinc ions, and *green surfaces* represent GFP tags. *Cyan arrows* in the beta cell indicate lateral diffusion of ZnT8 from the insulin granule to the surface membrane, *red arrows* indicate zinc transport or secretion, the *magenta arrow* indicates insulin secretion, and *magenta bars* indicate insulin molecules. *B*, anti-GFP and anti-FLAG Western blotting analysis of stably transfected INS-1E cells expressing ZnT8-GFP or ZnT8-FLAG/GFP and non-transfected INS-1E cells as indicated. A *red arrow* indicates positions of tagged ZnT8 between the 50–75-kDa markers. *C*, anti-ZnT8 Western blotting analysis of INS-1E (*left panel*) and HEK293 cells (*right panel*). Each panel consists of three lanes corresponding to stably transfected cells expressing ZnT8-GFP or ZnT8-FLAG/GFP and a non-transfected negative control as indicated. A *blue arrow* indicates the position of endogenous ZnT8 below the 50-kDa marker. A small protein band shift is noted between ZnT8-GFP and ZnT8-FLAG/GFP due to the FLAG-tag insertion.

the anti-ZnT8 antibody recognized a linear peptide epitope at the cytosolic N terminus, the presence of FLAG tag on the extracellular surface or GFP tag at the C terminus was unlikely to affect anti-ZnT8 immunoblotting. This assumption was confirmed experimentally with stably transfected HEK293 cells expressing ZnT8-GFP and ZnT8-FLAG/GFP. Both tagged ZnT8 variants in HEK293 cells yielded positive anti-ZnT8 immunoreactivities on the Western blot, but endogenous ZnT8 was not detected (*right panel*, Fig. 1*C*). The lack of the endogenous ZnT8 signal in HEK293 cells was consistent with cell-specific expression of ZnT8 restricted to pancreatic beta cells. Taken together, our results indicated that FLAG and GFP tagging did not affect anti-ZnT8 immunodetection. The low ZnT8-GFP and ZnT8-FLAG/GFP signals observed in stably transfected INS-1E cells (*left panel*, Fig. 1*C*) suggested that the expression levels of both tagged-ZnT8 variants were negligible relative to that of endogenous ZnT8.

Stable Antibody Complexes—The dual epitope-paratope recognition and interlock binding in the predicted antibody-ZnT8 complex (Fig. 1*A*) were expected to yield higher binding affinity

and a degree of conformation specificity. We tested a rabbit polyclonal (pAb) and a mouse monoclonal (mAb) anti-FLAG antibody for binding stability and specificity. FSEC analysis of detergent extracts of stably transfected INS-1E cells showed that both anti-FLAG pAb and mAb shifted the ZnT8-FLAG/GFP peak from an unbound position at 14.5 min (*red arrows*, Fig. 2*A*) to a complex position at 13.5 min (*purple arrows*). The difference between the apparent molecular masses of these two peak positions was ~150 kDa, corresponding to a 1-to-1 antibody-to-ZnT8 binding (Fig. 1*A*). As a negative control, neither anti-FLAG pAb nor mAb was found to cause any detectable change to the peak position of ZnT8-GFP (Fig. 2*A*), indicating that the observed peak shift was specific to the FLAG epitope.

Visualizing ZnT8 Surface Display—Confocal microscopy imaging of GFP fluorescence in live stably transfected INS-1E cells showed that ZnT8-FLAG/GFP or ZnT8-GFP was mainly confined intracellularly, but occasional ring-like GFP fluorescence was observed around the cell outer boundaries (Fig. 2*C*). Rabbit anti-FLAG pAb or mouse anti-FLAG mAb labeling to stable ZnT8-FLAG/GFP transfectants followed by staining with a red fluorophore-conjugated anti-rabbit or anti-mouse secondary antibody yielded discrete red puncta around the surface of INS-1E cells (Fig. 2, *B* and *D*). The surface staining was specific to the FLAG tag because no surface staining was detected on INS-1E cells stably expressing ZnT8-GFP (Fig. 2, *C* and *E*). The specificity of anti-FLAG staining was further supported by mutual inhibitions of rabbit anti-FLAG pAb and mouse anti-FLAG mAb labeling to the same FLAG epitope on the cell surface.

Quantifying ZnT8 Surface Display—To extend the imaging analysis of individual cells to the bulk cell population, we analyzed ZnT8-FLAG/GFP surface display by flow cytometry coupled with fluorescence-activated cell sorting (FACS) of stably transfected INS-1E cells over 10 million live cell counting events (Fig. 3*A*). Cellular GFP fluorescence and surface anti-FLAG staining exhibited >1000- and 100-fold fluorescence increases above the respective autofluorescence background (Fig. 3*A*). Three distinct cell populations were observed on the GFP fluorescence scale (*x* axis); cells in *red boxes* with mid-range GFP intensity showed a large spread of anti-FLAG fluorescence intensity on the *y* axis, whereas the low or high GFP cells in *orange* or *blue boxes* displayed limited anti-FLAG changes at a basal level (Fig. 3*A*). Thus, the mid-GFP cells were further gated into four subpopulations with increasing intensities of surface anti-FLAG staining (*red boxes*, Fig. 3*A*). All GFP-positive stable transfectants were sorted into six cell populations (*group 1–6*) (Fig. 3*A*). The post-FACS cells were solubilized by detergent and then analyzed by FSEC, showing a major ZnT8-FLAG/GFP peak (*red arrows*, Fig. 3*B*) in the mid-GFP population (*group 2–5*). A minor GFP fluorescence peak (*blue arrows*, Fig. 3*B*) with an apparent molecular mass of a GFP monomer (~30 kDa) was eluted after the main ZnT8-FLAG/GFP peak. This GFP peak was also observed in low and high GFP populations, but the peak height of the high GFP cells (*box 6*) was >1000-fold higher than that of low-GFP cells (*box 1*) (Fig. 3*B*). This dramatic difference in the cellular GFP amount was confirmed by the observation of exceedingly bright GFP fluorescence in high GFP cells using confocal microscopy.

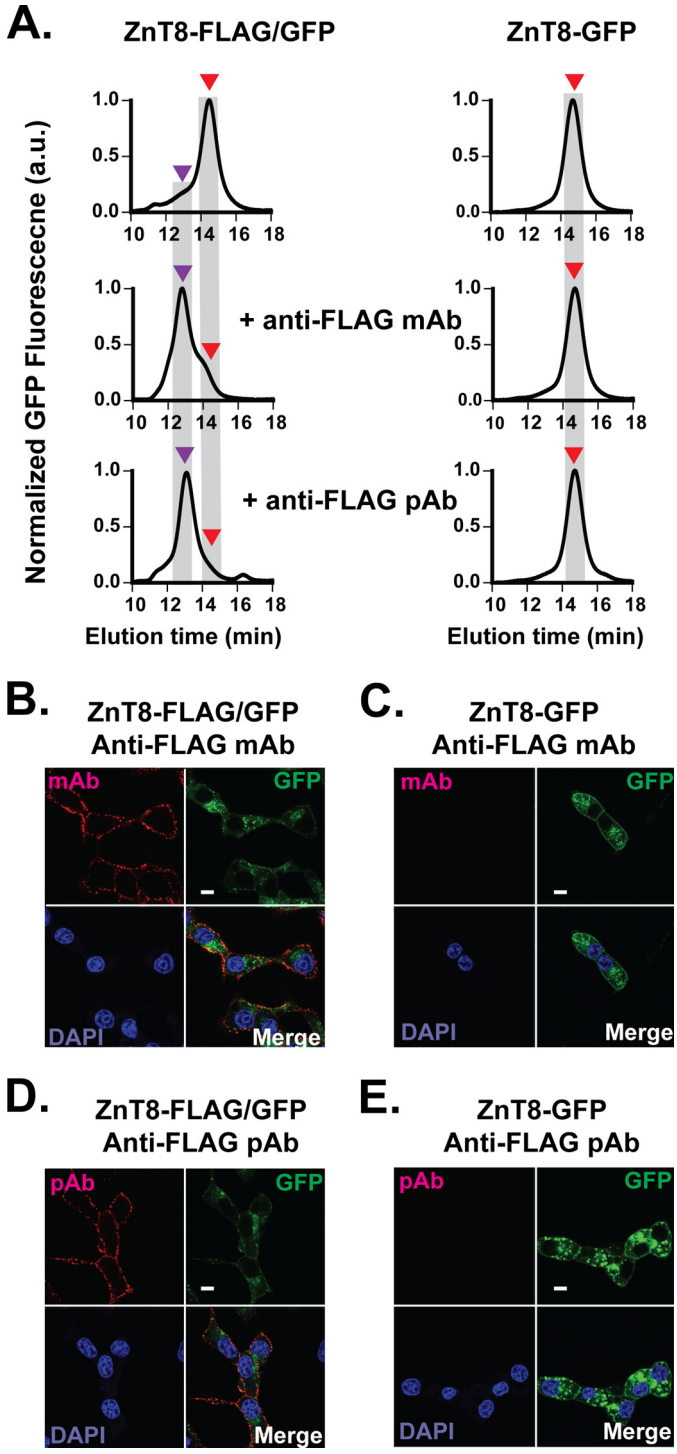

FIGURE 2. **Stable ZnT8-antibody complex and specific cell surface antibody labeling.** *A*, GFP-FSEC profiles of ZnT8-FLAG/GFP (*left panel*) and ZnT8-GFP (*right panel*) before and after the addition of anti-FLAG mAb or anti-FLAG pAb as labeled. *Red* and *purple arrows* indicate the peak positions of unbound ZnT8-FLAG/GFP and ZnT8-FLAG/GFP-antibody complex, respectively. *B–E*, representative immunofluorescence confocal images of stably transfected INS-1E cells expressing ZnT8-FLAG/GFP (*B* and *D*) or ZnT8-GFP (*C* and *E*). *Red*, cell surface staining by anti-FLAG mAb or anti-FLAG pAb. *Green*, GFP fluorescence. *Blue*, DAPI staining. *Red-green-blue* or *green-blue*, image merge. *Scale bar*, 15 μm. *a.u.*, arbitrary units.

Despite a complete loss of the ZnT8-FLAG/GFP protein in high-GFP cells (Fig. 3*B*), only the full-length *ZnT8-FLAG/GFP* mRNA was detected by RT-PCR, suggesting that the large GFP

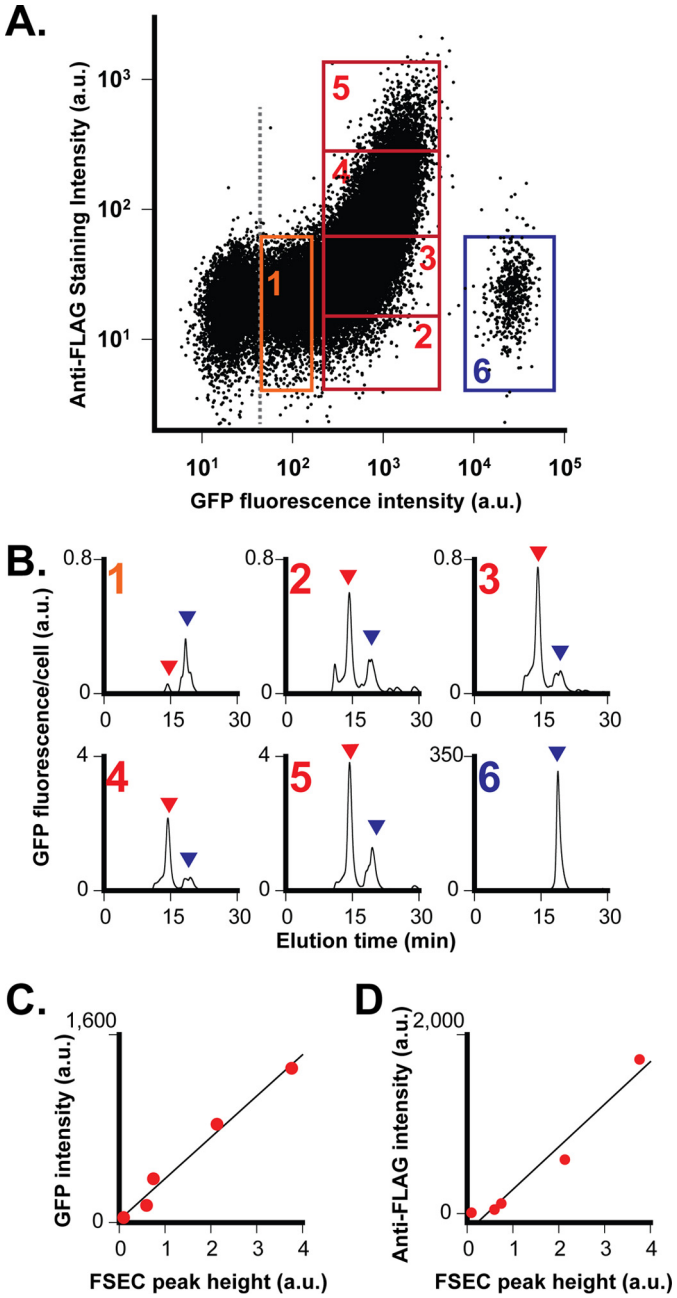

FIGURE 3. **Flow cytometry and FSEC analysis of stably transfected INS-1E cells.** *A*, bivariate flow cytometric analysis of cellular GFP intensity *versus* cell surface anti-FLAG staining intensity in a dot-plot format. Live stably transfected INS-1E cells expressing ZnT8-FLAG/GFP were labeled with anti-FLAG pAb and then gated for sorting into six subpopulations using window settings as numbered. An additional GFP gate (*gray dash line*) was applied to exclude GFP-negative cells. *B*, FSEC analysis of sorted populations as numbered in *A*. *Red* and *blue arrows* indicate ZnT8-FLAG/GFP and GFP peaks, respectively. The GFP fluorescence was normalized to the number of cells in each gated population. *C*, linear correlation between the peak height of ZnT8-FLAG/GFP from *B* and mean GFP intensity within the corresponding gate from *A*. The *solid line* represents a linear regression of five data points (r = 0.98). *D*, linear correlation between the peak height of ZnT8-FLAG/GFP from *B* and mean anti-FLAG staining intensity from *A*. The *solid line* represents a linear regression of five data points (r = 0.96). *a.u.*, arbitrary units.

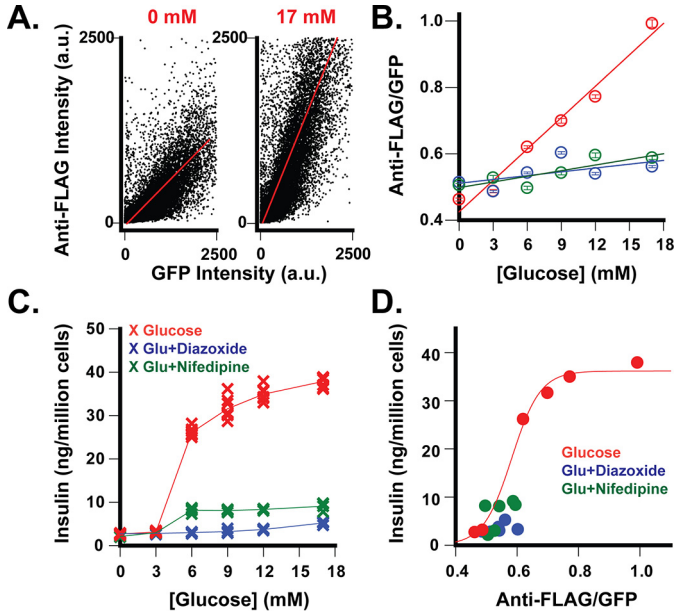

FIGURE 4. **GSIS-dependent ZnT8-FLAG/GFP surface display.** *A*, representative data of flow cytometric analysis of mid-GFP cells corresponding to gated populations 2–5 in Fig. 3*A*. The dot-plot shows an overall quasilinear relationship between cellular GFP intensity and cell surface anti-FLAG staining at 0 or 17 mM glucose as indicated. The *solid red lines* represent linear regressions of all counting events in dot-plots (r = 0.63–0.75). *B*, glucose-stimulated surface display of ZnT8-FLAG/GFP. The anti-FLAG/GFP ratio is plotted as a function of the glucose concentration. *Red*, glucose alone; *blue*, glucose plus 200 μM diazoxide; *green*, glucose plus 20 μM nifedipine. Data are the means ± S.E. from linear regression of over 10,000 counting events from 1 representative dataset of 4–8 independent experiments. *Solid lines* represent linear regression of the data points (r = 0.98). *C*, glucose-stimulated insulin secretion. Insulin secretion from replicated cells used for flow cytometric analysis was measured in the absence (*red*) or presence of diazoxide (*blue*) or nifedipine (*green*) and plotted as a function of the glucose concentration. Data were merged from 4–8 independent experiments. *D*, correlation between ZnT8-FLAG/GFP surface display and GSIS. The *solid line* represents a sigmoidal fit using corresponding data points in *B* and *C* as *x*- and y-variable, respectively (r = 0.99). *a.u.*, arbitrary units.

buildup in high GFP cells was a result of proteolytic degradation of the ZnT8-FLAG/GFP protein as opposed to an overexpression of GFP from a truncated *ZnT8*-FLAG/*GFP* genomic sequence. Because the GFP signal in high GFP cells was irrelevant to the cellular ZnT8-FLAG/GFP protein level, this population (3–4% of total cells) was excluded from analysis. Fluorescence data corresponding to each of the five sorted cell populations (group 1–5) were used to construct calibration curves that correlated the FSEC peak height to the fluorescence intensity of cellular GFP (Fig. 4*C*) or cell surface anti-FLAG staining (Fig. 4*D*). The linear correlations between the level of ZnT8-FLAG/GFP expression (FSEC peak height) with cellular GFP signal and surface anti-FLAG staining validated the linear responsiveness of flow cytometry measurements.

Correlating Surface Display and GSIS—About 60–70% of stably transfected INS-1E cells belonged to the mid-GFP population. Although ZnT8-FLAG/GFP expression varied among individual INS-1E cells, the bivariate flow cytometric profiles in Fig. 4*A* showed that the surface staining intensity of ZnT8-FLAG/GFP increased linearly with the GFP intensity of cellular ZnT8-FLAG/GFP expression. Thus, the anti-FLAG/GFP ratio obtained from a linear regression analysis over the entire mid-GFP population was used to normalize surface-displayed ZnT8-FLAG/GFP to total cellular ZnT8-FLAG/GFP expression (Fig. 4*A*). Mid-GFP cells were exposed to a series of glucose concentrations ranging from 0 to 17 mM, exhibiting a linear increase of the anti-FLAG/GFP ratio with the glucose concen-

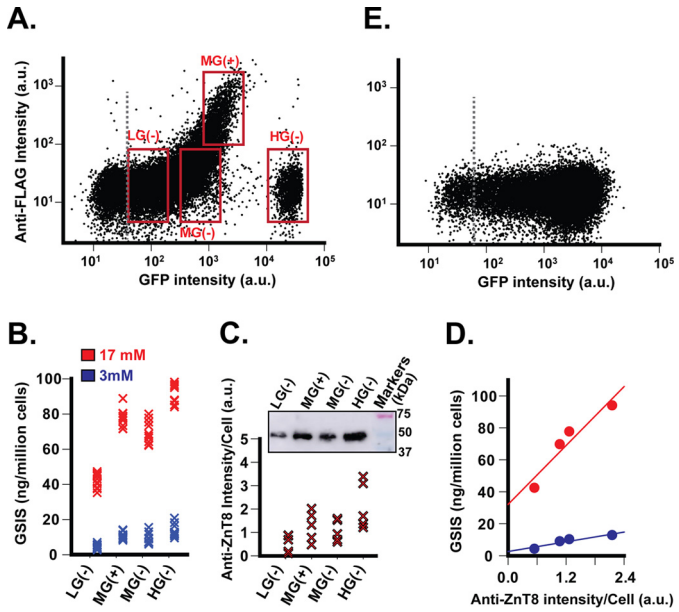

FIGURE 5. **Sorting insulin hypersecreting cells.** *A*, flow cytometric gates for cell fractionation. Stably transfected INS-1E cells expressing ZnT8-FLAG/GFP were gated with four window settings as marked in the dot-plot and sorted into low (LG(−)), middle (MG(+)), MG(−), and high (HG(−)) fractions as indicated. *B*, insulin secretion of the sorted cell populations in response to glucose stimulation at 3 (*blue*) or 17 mM (*red*). *C*, endogenous ZnT8 expression in the corresponding sorted cell populations. The cellular ZnT8 level was estimated by anti-ZnT8 immunoblotting normalized to the cell count. Data were merged from five independent experiments. *D*, correlation between endogenous ZnT8 expression and GSIS phenotype. *Solid lines* represent linear regressions of corresponding data points from *C* and *B* as *x* and *y* variables, respectively. *E*, dot-plot of stably transfected INS-1E cells expressing ZnT8-GFP with anti-FLAG labeling. *a.u.*, arbitrary units.

tration (Fig. 4*B*). The ratio at 17 mM glucose was 2.2-fold above a basal level at 0 mM glucose. GSIS from replicated cells was measured over the same glucose concentration range, showing a typical glucose-dependent GSIS profile (Fig. 4*C*). Two GSIS blockers, diazoxide and nifedipine (35, 36), were found to inhibit ZnT8-FLAG/GFP surface display at stimulatory glucose concentrations but had little effect at the basal glucose level (Fig. 4*B*). Concomitantly, both diazoxide and nifedipine inhibited GSIS without significant effects on the basal insulin release (Fig. 4*C*). The parallel inhibitory effects of diazoxide and nifedipine linked the ZnT8 surface display to GSIS. Plotting anti-FLAG/GFP ratios obtained at various glucose concentrations *versus* corresponding GSIS levels revealed a sigmoidal relationship between ZnT8-FLAG/GFP surface display and insulin secretion (Fig. 4*D*).

Sorting Hypersecreting Phenotype—Next we explored the possibility of sorting GSIS phenotype based on surface anti-FLAG staining. Live stably transfected INS-1E cells were labeled and sorted into four populations using the following window settings: mid-GFP with anti-FLAG (+) or (−), low or high GFP with anti-FLAG (−) (Fig. 5*A*). The sorted cells were reseeded and grown to confluence and then subjected to GSIS. The mid-GFP cells exhibited a small difference in GSIS between the anti-FLAG positive and negative cells (Fig. 5*B*), suggesting that these two populations shared a similar GSIS phenotype despite a large difference in surface anti-FLAG staining (Fig. 5*A*). Also, anti-ZnT8 immunoblotting analysis revealed a similar level of endogenous ZnT8 expression between the MG(+) and MG(−) population (Fig. 5*C*). On the other hand, low and high GFP cells (*LG(−)* and *HG(−)*), although both anti-FLAG-negative, exhibited a 2.3-fold difference in GSIS at a stimulatory glucose concentration of 17 mM (Fig. 5*B*). The hypersecreting phenotype of high GFP cells was accompanied by a 4.6-fold increase in endogenous ZnT8 expression over that of low GFP cells (Fig. 5*C*). Plotting the level of the endogenous ZnT8 expression in each of four sorted cell populations against the corresponding GSIS level revealed strong correlations between the endogenous ZnT8 level and GSIS either at a basal ($r = 0.90$) or a stimulatory ($r = 0.91$) glucose concentration (Fig. 5*D*). This result suggested that the GSIS phenotype was reliant on endogenous ZnT8 expression but independent of surface anti-FLAG staining. This observation may be explained by a high level of endogenous ZnT8 expression overriding any phenotypic perturbation of GSIS caused by a negligible level of ZnT8-FLAG/GFP expression (*left panel*, Fig. 1*C*). The hypersecreting beta cells were <5% of total cells, forming a distinct population cluster in the bivariate dot-plot (Fig. 5*A*). As a negative control, anti-FLAG labeling to stably transfected ZnT8-GFP INS-1E cells yielded a continuous GFP fluorescence distribution along the *x* axis (Fig. 5*E*). A discrete hypersecreting subpopulation was not observed.

Quantifying Endogenous ZnT8 on the Cell Surface—To detect the surface display of endogenous ZnT8, we biotinylated live INS-1E cells using a membrane impermeant, amine-reactive, and thiol-cleavable Sulfo-NHS-SS-Biotin. The resultant biotinylated surface proteins were detergent-solubilized, immobilized to streptavidin-conjugated magnetic beads, and then eluted by DTT. Immunoblotting detection of bound (biotinylated) or unbound (non-biotinylated) proteins in the cell lysate showed that Na^+/K^+ ATPase, a housekeeping cell surface marker, was completely captured by the beads and appeared in the eluate (Fig. 6*A*), whereas tubulin, an intracellular marker, was only observed in the unbound fraction (Fig. 6*B*). These control experiments indicated that Na^+/K^+ ATPase was fully biotinylated, whereas tubulin was fully protected from biotinylation by the cell surface membrane. Thus, the surface biotinylation reactions were complete and leakage-free. Anti-ZnT8 immunoblotting showed that a large majority of endogenous ZnT8 remained unbiotinylated. Only a small fraction (~1%) of endogenous ZnT8 was biotinylated, captured by the beads, and appeared in the eluate (Fig. 6*C*). To quantitatively compare the level of surface-displayed ZnT8 to Na^+/K^+ ATPase, we indiscriminately captured all biotinylated surface proteins and then selectively detected the immobilized ZnT8 or Na^+/K^+ ATPase using a respective rabbit anti-ZnT8 or rabbit anti-ATPase primary antibody followed by ELISA quantification using an identical anti-rabbit secondary antibody conjugated with horse radish peroxidase (HRP). Biotinylation on the protein extracellular surface did not affect antibody binding to the cytosolic epitopes and antibody-to-protein binding stoichiometry, allowing a quantitative comparison of HRP readouts despite a potential difference in the number of biotinylation sites on the extracellular surface of ZnT8 and Na^+/K^+ ATPase. HRP readouts of serial dilutions of biotinylated proteins were used to generate anti-ZnT8 standard curves (Fig. 6 D), and the -fold difference between biotinylated ZnT8 and Na^+/K^+

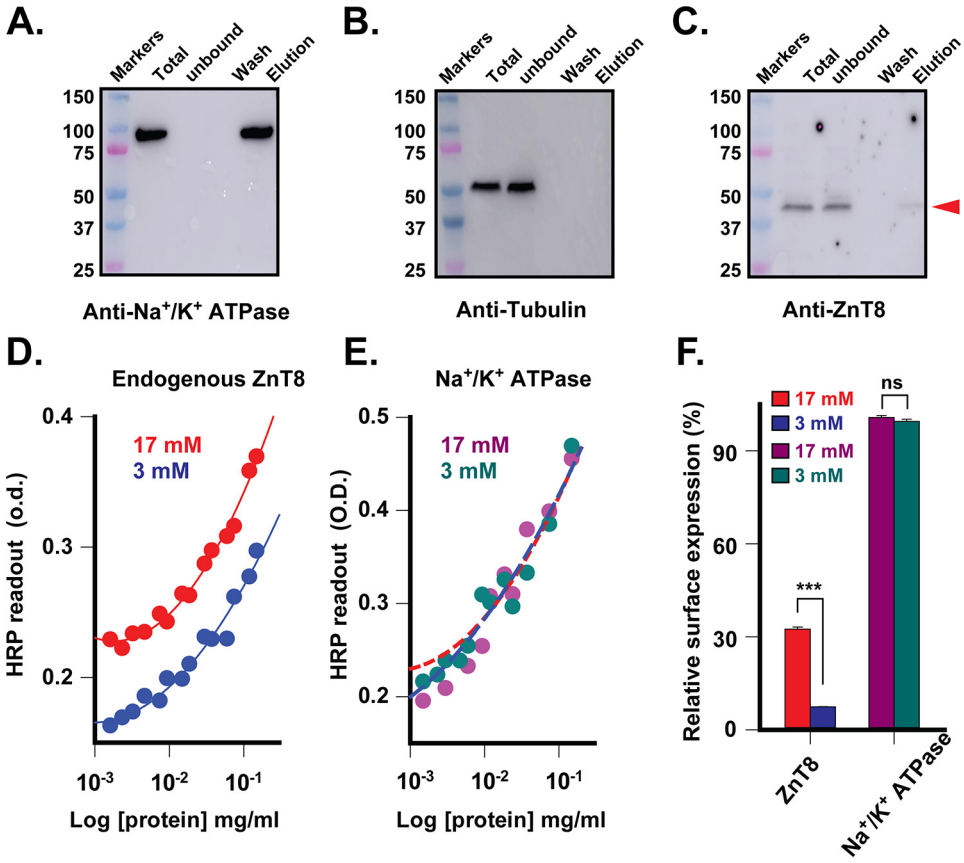

FIGURE 6. **GSIS-dependent surface display of endogenous ZnT8.** *A–C*, anti-Na^+/K^+ ATPase, anti-tubulin, and anti-ZnT8 Western blotting analysis of surface biotinylation of live INS-1E cells. Biotinylated proteins were captured by streptavidin-coated magnetic beads, washed, and then eluted for immunoblotting analysis using a respective primary antibody as indicated. The *red arrow* indicates endogenous ZnT8. *D*, ELISA readouts of surface displayed ZnT8 on INS-1E cells that were exposed to 3 (*blue*) or 17 mM (*red*) glucose. *Solid lines* are standard curves generated by least squares fits of serial dilution data points to a second order logarithmic equation. *E*, quantification of surface-displayed ZnT8. Anti-Na^+/K^+ ATPase ELISA readouts are shown for serial dilutions of the identical cell lysate used in *D*. *Magenta* or *dark cyan circles* are anti-Na^+/K^+ ATPase readouts measured with 17 or 3 mM glucose. *Dashed lines* are least square fits of anti-ZnT8 standard curves in *D* to the anti-Na^+/K^+ ATPase data points using the -fold difference between biotinylated ZnT8 and Na^+/K^+ ATPase as a fitting parameter. *Red* or *blue dash lines* show the fit of 17 or 3 mM glucose data points. *F*, glucose-stimulated ZnT8 surface display. The values of relative surface expression were obtained from *E* in reference to the average level of the housekeeping Na^+/K^+ ATPase. *Bars* are the means ± S.E. from least-squares fitting (*ns*, $p > 0.1$; ***, $p < 0.001$).

ATPase was obtained by least squares fitting of an anti-ZnT8 standard curve to anti-Na^+/K^+ ATPase readouts (Fig. 6*E*). The surface-displayed endogenous ZnT8 was determined to be 7.5 ± 0.1% and 32.5 ± 0.7% that of the Na^+/K^+ ATPase level when the live INS-1E cells were biotinylated in the presence of 3 and 17 mM glucose, respectively (Fig. 6*F*). Glucose stimulation at 17 mM did not affect the level of surface Na^+/K^+ ATPase (Fig. 6*E*) but increased surface-displayed ZnT8 by 4.4-fold, as shown by an upward shift of the anti-ZnT8 standard curve (Fig. 6*D*).

Discussion

At the mRNA level ZnT8 is by far the highest expressed zinc transporter in pancreatic tissues at a level comparable with β-actin (10). Although surface-displayed ZnT8 was estimated to be ~1% that of total ZnT8 in INS-1E cells, the abundant expression of ZnT8 in beta cells equated this small percentage with 7.5% of surface Na^+/K^+ ATPase at a basal glucose concentration. Glucose stimulation further increased surface displayed ZnT8 to 32.5%. The abundant presence of surface ZnT8 and its strong responsiveness to glucose stimulation suggest that ZnT8 could be a significant target of humoral autoantibodies. The Y-shaped molecular architecture of ZnT8 appears inherently prone to $(Fab)_2$ binding, whereas the Fc region of the bound autoantibody is capable of binding immune effector cells to trigger antibody-dependent cellular cytotoxicity against the opsonized beta cells. The finding of the GSIS-dependent ZnT8 surface display raises the possibility of a potential pathological role of ZnT8 self-antigen in humoral autoimmunity that may contribute to a positive feedback loop of beta cell destruction.

In a differentiated beta cell, zinc is co-packaged and co-secreted with insulin, providing a natural biomarker for insulin biosynthesis and GSIS. Zinc-containing granules are found in a number of neurosecretory cells, each utilizing a specialized zinc transporter for vesicular zinc sequestration (9). Among vesicular zinc transporters, ZnT8 is almost exclusively expressed in pancreatic islets. Using a FLAG-tagged ZnT8 variant and specific anti-FLAG surface labeling, we developed a quantitative analysis of ZnT8 surfacing in live beta cells and correlated the change in ZnT8 surface display to the GSIS phenotype. For a major population of stable INS-1E transfectants with a relatively homogenous GSIS phenotype (the mid-GFP population), changes in ZnT8-FLAG/GFP surface display were found parallel to changes in insulin secretion in response to glucose stim-

ulation or diazoxide/nifedipine inhibition (Fig. 4). This correlation demonstrated the predictive potential of ZnT8 surface display for regulated insulin secretion. For minor cell populations with heterogeneous GSIS phenotypes, the detection of hypersecreting INS-1E cells (the high GFP population) in <5% of total INS-1E cells demonstrated the sensitivity of ZnT8 as a surface biomarker for FACS (Fig. 5*A*). This small cell population could be readily isolated from the bulk cell culture by FACS after specific antibody labeling to surface displayed ZnT8-FLAG/GFP.

The stably expressed ZnT8-FLAG/GFP was found negligible in quantity as compared with the endogenous ZnT8 (*left panel*, Fig. 1*C*). A minute amount of ZnT8-FLAG/GFP expression appeared to have no significant phenotypic effect; that is, the GSIS activity of sorted cells was independent of anti-FLAG staining but positively correlated with an increasing level of endogenous ZnT8 (Fig. 5*D*). This finding mirrored decreased GSIS phenotypes in pancreatic beta cells after siRNA-mediated inhibition of endogenous *ZnT8* expression (5, 37, 38), suggesting that the increased endogenous ZnT8 level may underlie the hypersecreting phenotype of the high GFP population. Because surface display and cellular expression of ZnT8-FLAG/GFP were linearly correlated (Fig. 4*A*), a similar correlation may be held for endogenous ZnT8, a fraction of which might move along the insulin secretory pathway to the surface membrane after insulin secretion. Thus, the level of surface displayed ZnT8 may be used to indicate the intracellular ZnT8 level, which in turn reflects the GSIS phenotype of pancreatic beta cells. This finding has motivated the development of conformation-specific anti-ZnT8 antibodies that are used to track and isolate functional beta cells in heterogeneous pancreatic tissues or in bulk cultures of human pancreatic progenitor cells in various differentiated states of GSIS phenotype.

Experimental Procedures

Expression Constructs—The human ZnT8 isoform-1 cDNA (NM173851.2) housed in a pCMV6-entry vector (OriGene Technologies) was shuttled into a mammalian expression vector pCMV6-AC-GFP with a C-terminal GFP tag. A FLAG tag was added to an extracellular loop between transmembrane helices 3 and 4. All constructs were confirmed by double strand DNA sequencing.

Stable Cell Lines—Clonal rat insulinoma INS-1E cells (passage 33–35, AddexBio, catalog #C0018009) were grown as monolayers in a humidified atmosphere with 5% CO_2 at 37 °C in complemented RMPI 1640 medium supplied with 10% (v/v) fetal bovine serum (FBS), 100 units/ml penicillin, 100 μg/ml streptomycin, 10 mM HEPES, 2 mM glutamine, 1 mM sodium pyruvate, and 50 μM 2-mercaptoethanol. For stable transfection, 12 μg of hZnT8-FLAG/GFP or hZnT8-GFP plasmid was transfected into INS-1E cells in a 10-cm dish at 90% confluence using Lipofectamine 2000^{TM} (Invitrogen) according to the manufacturer's instructions. About 48 h after transfection, cells were passaged at a 1:10 split ratio. At this time, G418 (Invitrogen) was added to 600 μg/ml. After 2 weeks of G418 selection, G418-resistant cells were sorted on a MoFlo XDP cell sorter (Beckman Coulter) to collect GFP-positive transfectants. The sorted cells were reseeded at a density of 1×10^6/35-mm dish with G418. Subcultures within five passages were used for all experiments.

Western Blotting—Stable expression INS-1E or HEK293 cells were resuspended in an assay buffer (100 mM NaCl, 20 mM HEPES, 2 mM tris(2-carboxyethyl)phosphine, pH 7.0), and lysed using an ice-chilled high pressure Microfluidizer. The cell membranes were collected by ultracentrifugation at 258,000 × *g* for 1 h and solubilized in assay buffer plus 1% SDS. 10–30 μg of solubilized protein was loaded to a 4–20% gradient miniprotean TGX gel (Bio-Rad). Human ZnT8-FLAG/GFP, human ZnT8-GPF, and endogenous rat ZnT8 were detected using 1:200 anti-FLAG (Sigma, catalog #F7425), 1:1000 anti-GFP (Origene, catalog #TA150041), 1:200 anti-ZnT8 (Proteintech, catalog #16169-I-AP) antibodies followed by 1:2000 anti-rabbit or anti-mouse HRP-conjugated secondary antibody (GE catalog #NA934V or NA931V). The protein bands on the immunoblots were recorded on Amersham Biosciences Imager 600 (GE Healthcare) and analyzed using ImageJ (National Institutes of Health).

FSEC—Stably transfected INS-1E cells were plated at a density of 0.5×10^6 per well in a 24-well plate. About 48 h after seeding, cells were washed once with ice-chilled assay buffer then solubilized using 200 μl of assay buffer plus 0.02% DDM. The detergent crude extract was centrifuged at 258,000 × *g* from 30 min. The resultant supernatant was injected into a TSKgel G3000SWXL size exclusion HPLC column (Tosoh Biosciences) pre-equilibrated with the assay buffer plus 0.02% DDM. The elution profile of GFP fluorescence was monitored using a fluorescence detector with excitation at 480 nm and emission at 515 nm (Shimadzu).

Immunofluorescence—Stable expression cells grown on coverslips at 50% confluence were preblocked using 1% BSA in Ca-PBS (Corning, catalog #2A030CV) for 30 min, then exposed to a primary rabbit anti-FLAG polyclonal or a mouse anti-FLAG monoclonal antibody (Sigma, catalog #F7425 or F3165), both diluted at a 1:100 ratio in 100 μl of culture medium. After a 2-h incubation in 37 °C, cells were washed with Ca-PBS, then exposed to Alexa Fluor-594-conjugated goat-anti-rabbit or goat-anti-mouse secondary antibody in 1:200 dilution with culture medium (Thermo Fisher, catalog #A11307 or A11032). After 30 min of incubation at 4 °C, cells were washed free of secondary antibody with Ca-PBS, then fixed with 4% paraformaldehyde. Nuclei were counterstained with DAPI. Cells were then imaged using a Zeiss LSM 700 inverted confocal microscope with a 100× oil objective. Fluorescence probes were excited by three separate laser lines (561, 405, and 488 nm) and monitored at the respective emission wavelength ranges under the control of Zen software (Zeiss).

Flow Cytometry—Flow cytometric analyses were performed on a MoFlo XDP cell sorter (Beckman Coulter) equipped with 488- and 640-nm lasers. Data were collected on forward scatter, side scatter, 530-nm and 670-nm fluorescence channels. For cell population analysis, stably transfected INS-1E cells expressing ZnT8-FLAG/GFP or ZnT8-GFP in 10-cm plates at 90% confluence were stained with anti-FLAG pAb (Sigma, catalog #F7425) in a 1:100 dilution for 2 h at 37 °C, washed with Hanks' balanced salt solution, then stained with Alexa Fluor-647-conjugated goat-anti-rabbit secondary antibody in a 1:200

dilution (Thermo Fisher, catalog #A21244) for 30 min at 4 °C. After surface staining, cells were trypsinized, counted, and resuspended in ice-chilled Hanks' balanced salt solution at a density of 1×10^6 cells/ml, and then flow cytometric analysis was conducted within 30 min. >99% of scattering events belonged to a singlet cell population with >98% cell viability based on propidium iodide staining analysis. A GFP fluorescence gate was set up to exclude GFP-negative cells based on the non-transfected INS-1E cell control. A bivariate dot-plot of cellular GFP intensity *versus* surface anti-FLAG staining intensity was displayed to define target population gates, which were applied to sort 10^7 cells into various cell fractions. Approximately equal number of sorted cells from each fraction ($\sim 0.5 \times 10^6$ cells) was reseeded in a 24-well plate, and the subculture was harvested 48 h later for FSEC analysis and anti-ZnT8 immunoblotting. For quantification of ZnT8-FLAG/GFP surface display and GSIS, a mid-GFP population gate was applied to sort stably transfected INS-1E cells expressing ZnT8-FLAG/GFP. Aliquots of post-FACS cells were reseeded in a 24-well plate at a density of 0.5×10^6 cells/well. After subculturing for 48 h, replicated cells in adherent cell culture were washed with a glucose-free Krebs-Ringer bicarbonate HEPES (KRBH) buffer containing 135 mM NaCl, 3.6 mM KCl, 5 mM $NaHCO_3$, 0.5 mM NaH_2PO_4, 0.5 mM $MgCl_2$, 1.5 mm $CaCl_2$, 10 mm HEPES, pH 7.4, and BSA 0.1%. The washed cells were starved in glucose-free KRBH buffer for 120 min at 37 °C, then exposed to various concentrations of glucose with or without 200 μM diazoxide or 20 μM nifedipine for 90 min in the presence of 1:100 primary anti-FLAG antibody (Sigma, catalog #F7425). The anti-FLAG-labeled cells were then washed with ice-cold KRBH, stained with 1:200 goat-anti-rabbit secondary antibody (Thermo Fisher, catalog #A21244) at 4 °C for 30 min, harvested in a single cell suspension, and subjected to flow cytometric analysis. The entire mid-GFP population was gated for linear regression analysis. The normalized ZnT8-FLAG/GFP surface labeling is presented as the ratio of anti-FLAG/GFP ± S.E. $n = \sim$10,000 live cells.

GSIS—Cells were plated in a 24-well plate at a density of 0.5×10^6 cells/well and grown in complemented RPMI medium with G418. After subculturing for 48 h, the cells were washed and starved as described above. Insulin secretion was induced for 90 min using increasing concentrations of glucose in the KRBH buffer. The secreted insulin was measured in triplicate using a sandwich immunoassay according to manufacturer's instructions (Cisbio, catalog #62INSPEB) on a Flexstation-3 microplate reader operating in homogeneous time resolved fluorescence (HTRF) mode (Molecular Dynamics). The number of cells in each well was counted and used to normalize the secreted insulin. The data are presented as the means ± S.E., $n = 4$ independent experiments.

Biotinylation Immunoblotting—Clonal INS-1E cells were plated at 2×10^6 cells/10 cm plate. About 48 h after seeding, cells were washed with Ca-PBS adjusted to pH 8.0. 1 mg of Sulfo-NHS-SS-Biotin powder (Thermo Fisher catalog # 21328) was dissolved in 1.7 ml of Ca-PBS, pH 8.0, and used immediately to overlay the cell monolayer with gentle shaking. After 10 min of incubation at 37 °C, cells were washed with 100 mM glycine in assay buffer, then solubilized with 400 μl of assay buffer plus 1% DDM. The detergent extract (~4 mg/ml) was incubated with 0.1 ml of streptavidin-conjugated magnetic beads (Thermo Fisher) and washed with assay buffer plus 0.1% DDM, and then the bound proteins were eluted using 40 μl of assay buffer plus 10 mM DTT and 4× Laemmli sample buffer (Bio-Rad, catalog #161-0747). 4 μl of solubilized proteins (total 16 μg) before and after bead binding, bead wash, and eluate (20 μl for anti-ZnT8, 0.4 μl for anti-Na^+/K^+ ATPase, and 1 μl for anti-tubulin immunoblotting) were loaded onto the gel. Na^+/K^+ ATPase, tubulin, and endogenous ZnT8 in the identical eluate were detected using 1:1000 anti-Na^+/K^+ ATPase (Abcam, catalog #7671), 1:1000 anti-tubulin (Thermo Fisher, catalog #322500), and 1:200 anti-ZnT8 antibody (Proteintech, catalog #16169-I-AP), respectively.

Biotinylation ELISA—About 2×10^6 clonal INS-1E cells in 10-cm plates were washed, starved, exposed to 3 or 17 mM glucose, and biotinylated as described above. The surface biotinylated cells were washed with 100 mM glycine in assay buffer, then overlaid with 20 μg NeutrAvidin (Thermo Fisher, catalog #31000) in Ca-PBS + 2% BSA. After 1 h of incubation at 37 °C, cells were washed free of unbound NeutrAvidin and solubilized in 0.4 ml of solubilization solution (PBS + 1% DDM with 0.5% ethanol-saturated PMSF). 2-Fold serial dilutions of the detergent extract were prepared, each added in 100 μl to a 96-well biotin-coated plate (Thermo Fisher, catalog #15151). After 1 h of incubation at room temperature, the immobilized biotinylated proteins in each well were washed with PBS + 2% BSA + 0.1% DDM, then incubated with 0.2 μg of anti-ZnT8 (Proteintech, catalog #16169-I-AP) or 0.2 μg of anti-Na^+/K^+ ATPase antibody (Abcam, catalog #58475) in 100 μl of TBS blocking solution plus 5% BSA (Thermo Fisher, catalog #37520). After a 2-h incubation at room temperature, the immobilized primary antibody was washed with TBS blocking solution, then incubated with 1:3000 HRP-conjugated anti-rabbit secondary antibody (Thermo Fisher, catalog #65-6120) in 100 μl of TBS-blocking solution plus 2% BSA for 30 min at room temperature. After a final wash with TBS blocking solution to remove unbound secondary antibody, the peroxidase was detected in triplicate using 100 μl of ABTS reaction solution per well (Thermo Fisher, catalog #002040). ELISA readouts were recorded at 415 nm on a Flexstation-3 microplate reader.

Data Analysis—Anti-ZnT8 HRP readouts of serial dilutions were plotted against the protein concentrations and fitted to a second order logarithm equation $y = y_o + a\ln x + b(\ln x)^2$, where y is the anti-ZnT8 HRP readout, and x is the protein concentration. Lease squares fit yielded three fitting parameters y_o, a, and b for each dataset obtained in 3 or 17 mM glucose. The fit results (standard curves) were shown as solid lines in Fig. 6*D*. To calculate the -fold difference (f) between ZnT8 and Na^+/K^+ ATPase in the identical detergent extract, anti-ZnT8 standard curves in Fig. 6*D* were fitted to anti-Na^+/K^+ ATPase HRP readouts using the equation $y = y_o + a\ln(f^*x) + b(\ln(f^*x))^2$, where y is anti-Na^+/K^+ ATPase HRP readouts, x is the protein concentration, y_o, a, and b are fixed constants derived from the anti-ZnT8 standard curve. Lease squares fit yielded one fitting parameter f for each dataset measured with 3 or 17 mM glucose. The fits were shown as *dash lines* in Fig. 6*E*. Fits of experimental

data were preformed using the data analysis software SIGMAPLOT (SPSS Inc.).

Homology Modeling—Protein sequences of the R-allele of human ZnT8 isoform-2 and *Escherichia coli* zinc transporter YiiP were aligned using MODELLER 9.16. The alignment was imported into Swiss model to generate a homolog model of ZnT8 using the crystal structure of YiiP at 2.9-Å resolution as a template (PDB accession number 3H90). The GFP and immunoglobin were modeled based on respective crystal structures (accession number 2G6Y and 1IGY) and docked manually to the ZnT8 homodimer. The graphic representation of the resulted complex model was prepared using PyMol (Delano Scientific).

Statistics—The difference between two groups was analyzed using unpaired Student's *t* test.

Author Contributions—D. F. conceived the idea and developed the assays with Q. H. and C. M. Q. H. performed the cell biology experiments. C. M. performed the biochemistry experiments. H. Z. assisted in the flow cytometry experiments. All authors contributed to the data analysis. D. F. wrote the paper with Q. H. and C. M.

Acknowledgments—The Zeiss confocal microscope was funded through National Institutes of Health shared instrumentation Grant S10OD016374. The MoFlo XDP cell sorter was funded through National Institutes of Health Grants S10OD016315 and S10RR13777001.

References

1. Rorsman, P., Eliasson, L., Renström, E., Gromada, J., Barg, S., and Göpel, S. (2000) The cell physiology of biphasic insulin secretion. *News Physiol. Sci.* **15,** 72–77
2. Eizirik, D. L., Colli, M. L., and Ortis, F. (2009) The role of inflammation in insulitis and beta cell loss in type 1 diabetes. *Nat. Rev. Endocrinol.* **5,** 219–226
3. Dunn, M. F. (2005) Zinc-ligand interactions modulate assembly and stability of the insulin hexamer: a review. *Biometals* **18,** 295–303
4. Dodson, G., and Steiner, D. (1998) The role of assembly in insulin's biosynthesis. *Curr. Opin. Struct. Biol.* **8,** 189–194
5. Fu, Y., Tian, W., Pratt, E. B., Dirling, L. B., Shyng, S. L., Meshul, C. K., and Cohen, D. M. (2009) Down-regulation of ZnT8 expression in INS-1 rat pancreatic beta cells reduces insulin content and glucose-inducible insulin secretion. *PLoS ONE* **4,** e5679
6. Lemaire, K., Ravier, M. A., Schraenen, A., Creemers, J. W., Van de Plas, R., Granvik, M., Van Lommel, L., Waelkens, E., Chimienti, F., Rutter, G. A., Gilon, P., in't Veld, P. A., and Schuit, F. C. (2009) Insulin crystallization depends on zinc transporter ZnT8 expression but is not required for normal glucose homeostasis in mice. *Proc. Natl. Acad. Sci. U.S.A.* **106,** 14872–14877
7. Nicolson, T. J., Bellomo, E. A., Wijesekara, N., Loder, M. K., Baldwin, J. M., Gyulkhandanyan, A. V., Koshkin, V., Tarasov, A. I., Carzaniga, R., Kronenberger, K., Taneja, T. K., da Silva Xavier, G., Libert, S., Froguel, P., Scharfmann, R., *et al.* (2009) Insulin storage and glucose homeostasis in mice null for the granule zinc transporter ZnT8 and studies of the type 2 diabetes-associated variants. *Diabetes* **58,** 2070–2083
8. Wijesekara, N., Dai, F. F., Hardy, A. B., Giglou, P. R., Bhattacharjee, A., Koshkin, V., Chimienti, F., Gaisano, H. Y., Rutter, G. A., and Wheeler, M. B. (2010) Beta cell-specific Znt8 deletion in mice causes marked defects in insulin processing, crystallisation and secretion. *Diabetologia* **53,** 1656–1668
9. Kambe, T. (2011) An overview of a wide range of functions of ZnT and Zip zinc transporters in the secretory pathway. *Biosci. Biotechnol. Biochem.* **75,** 1036–1043
10. Lemaire, K., Chimienti, F., and Schuit, F. (2012) Zinc transporters and their role in the pancreatic beta cell. *J. Diabetes Investig.* **3,** 202–211
11. Chimienti, F., Devergnas, S., Favier, A., and Seve, M. (2004) Identification and cloning of a beta cell-specific zinc transporter, ZnT-8, localized into insulin secretory granules. *Diabetes* **53,** 2330–2337
12. Foster, M. C., Leapman, R. D., Li, M. X., and Atwater, I. (1993) Elemental composition of secretory granules in pancreatic islets of Langerhans. *Biophys. J.* **64,** 525–532
13. Gyulkhandanyan, A. V., Lu, H., Lee, S. C., Bhattacharjee, A., Wijesekara, N., Fox, J. E., MacDonald, P. E., Chimienti, F., Dai, F. F., and Wheeler, M. B. (2008) Investigation of transport mechanisms and regulation of intracellular Zn^{2+} in pancreatic alpha cells. *J. Biol. Chem.* **283,** 10184–10197
14. Murgia, C., Devirgiliis, C., Mancini, E., Donadel, G., Zalewski, P., and Perozzi, G. (2009) Diabetes-linked zinc transporter ZnT8 is a homodimeric protein expressed by distinct rodent endocrine cell types in the pancreas and other glands. *Nutr. Metab. Cardiovasc. Dis.* **19,** 431–439
15. Tamaki, M., Fujitani, Y., Uchida, T., Hirose, T., Kawamori, R., and Watada, H. (2009) Downregulation of ZnT8 expression in pancreatic beta cells of diabetic mice. *Islets* **1,** 124–128
16. Hou, J. C., Min, L., and Pessin, J. E. (2009) Insulin granule biogenesis, trafficking, and exocytosis. *Vitam. Horm.* **80,** 473–506
17. Tsuboi, T., and Rutter, G. A. (2003) Insulin secretion by 'kiss-and-run' exocytosis in clonal pancreatic islet beta cells. *Biochem. Soc. Trans.* **31,** 833–836
18. Vo, Y. P., Hutton, J. C., and Angleson, J. K. (2004) Recycling of the dense-core vesicle membrane protein phogrin in Min6 beta cells. *Biochem. Biophys. Res. Commun.* **324,** 1004–1010
19. Arvan, P., Pietropaolo, M., Ostrov, D., and Rhodes, C. J. (2012) Islet autoantigens: structure, function, localization, and regulation. *Cold Spring Harb. Perspect. Med.* **2,** a007658
20. Mauvais, F. X., Diana, J., and van Endert, P. (2016) Beta cell antigens in type 1 diabetes: triggers in pathogenesis and therapeutic targets. *F1000Res* 10.12688/f1000research.7411.1
21. Roep, B. O., and Peakman, M. (2012) Antigen targets of type 1 diabetes autoimmunity. *Cold Spring Harb. Perspect. Med.* 2, a007781
22. Bettini, M., and Vignali, D. A. (2011) T cell-driven initiation and propagation of autoimmune diabetes. *Curr. Opin. Immunol.* **23,** 754–760
23. Chujo, D., Foucat, E., Nguyen, T. S., Chaussabel, D., Banchereau, J., and Ueno, H. (2013) ZnT8-specific CD4+ T cells display distinct cytokine expression profiles between type 1 diabetes patients and healthy adults. *PLoS ONE* **8,** e55595
24. Dang, M., Rockell, J., Wagner, R., Wenzlau, J. M., Yu, L., Hutton, J. C., Gottlieb, P. A., and Davidson, H. W. (2011) Human type 1 diabetes is associated with T cell autoimmunity to zinc transporter 8. *J. Immunol.* **186,** 6056–6063
25. Énée, É., Kratzer, R., Arnoux, J. B., Barilleau, E., Hamel, Y., Marchi, C., Beltrand, J., Michaud, B., Chatenoud, L., Robert, J. J., and van Endert, P. (2012) ZnT8 is a major CD8+ T cell-recognized autoantigen in pediatric type 1 diabetes. *Diabetes* **61,** 1779–1784
26. Hamel, Y., Mauvais, F. X., Pham, H. P., Kratzer, R., Marchi, C., Barilleau, É., Waeckel-Enée, E., Arnoux, J. B., Hartemann, A., Cordier, C., Mégret, J., Rocha, B., de Lonlay, P., Beltrand, J., Six, A., Robert, J. J., and van Endert, P. (2016) A unique CD8(+) T lymphocyte signature in pediatric type 1 diabetes. *J. Autoimmun.* **73,** 54–63
27. Yu, C., Burns, J. C., Robinson, W. H., Utz, P. J., Ho, P. P., Steinman, L., and Frey, A. B. (2016) Identification of candidate tolerogenic CD8(+) T cell epitopes for therapy of Type 1 diabetes in the NOD mouse model. *J. Diabetes Res.* **2016,** 9083103
28. Wenzlau, J. M., Juhl, K., Yu, L., Moua, O., Sarkar, S. A., Gottlieb, P., Rewers, M., Eisenbarth, G. S., Jensen, J., Davidson, H. W., and Hutton, J. C. (2007) The cation efflux transporter ZnT8 (Slc30A8) is a major autoantigen in human type 1 diabetes. *Proc. Natl. Acad. Sci. U.S.A.* **104,** 17040–17045
29. Atkinson, M. A., Bluestone, J. A., Eisenbarth, G. S., Hebrok, M., Herold, K. C., Accili, D., Pietropaolo, M., Arvan, P. R., Von Herrath, M., Markel, D. S., and Rhodes, C. J. (2011) How does type 1 diabetes develop? The notion of homicide or beta cell suicide revisited. *Diabetes* **60,** 1370–1379
30. Merglen, A., Theander, S., Rubi, B., Chaffard, G., Wollheim, C. B., and Maechler, P. (2004) Glucose sensitivity and metabolism-secretion cou-

pling studied during two-year continuous culture in INS-1E insulinoma cells. *Endocrinology* **145,** 667–678
31. Lu, M., Chai, J., and Fu, D. (2009) Structural basis for autoregulation of the zinc transporter YiiP. *Nat. Struct. Mol. Biol.* **16,** 1063–1067
32. Lu, M., and Fu, D. (2007) Structure of the zinc transporter YiiP. *Science* **317,** 1746–1748
33. Shaner, N. C., Lambert, G. G., Chammas, A., Ni, Y., Cranfill, P. J., Baird, M. A., Sell, B. R., Allen, J. R., Day, R. N., Israelsson, M., Davidson, M. W., and Wang, J. (2013) A bright monomeric green fluorescent protein derived from Branchiostoma lanceolatum. *Nat. Methods* **10,** 407–409
34. Merriman, C., Huang, Q., Rutter, G. A., and Fu, D. (2016) Lipid-tuned zinc transport activity of human znt8 protein correlates with risk for type-2 diabetes. *J. Biol. Chem.* **291,** 26950–26957
35. Mariot, P., Gilon, P., Nenquin, M., and Henquin, J. C. (1998) Tolbutamide and diazoxide influence insulin secretion by changing the concentration but not the action of cytoplasmic Ca2+ in beta cells. *Diabetes* **47,** 365–373
36. Doyle, M. E., and Egan, J. M. (2003) Pharmacological agents that directly modulate insulin secretion. *Pharmacol. Rev.* **55,** 105–131
37. Petersen, A. B., Smidt, K., Magnusson, N. E., Moore, F., Egefjord, L., and Rungby, J. (2011) siRNA-mediated knock-down of ZnT3 and ZnT8 affects production and secretion of insulin and apoptosis in INS-1E cells. *APMIS* **119,** 93–102
38. El Muayed, M., Billings, L. K., Raja, M. R., Zhang, X., Park, P. J., Newman, M. V., Kaufman, D. B., O'Halloran, T. V., and Lowe, W. L., Jr. (2010) Acute cytokine-mediated down-regulation of the zinc transporter ZnT8 alters pancreatic beta cell function. *J. Endocrinol.* **206,** 159–169